

# Bouncing Oil Droplets as a Macroscopic Model of Single-Particle Diffraction

by

Trent Jones

Submitted in Partial Fulfillment of the  
Requirements for the Degree

*Bachelor of Arts*

Supervised by  
Dr. Daniel Borrero-Echeverry

Department of Physics

Willamette University, College of Liberal Arts  
Salem, Oregon

2019

## Presentations and publications

- April, 2018. Willamette University ATEP Oral Presentation - “Modeling Single-Particle Diffraction with Bouncing Droplets.”
- September, 2018. Willamette University SCRP Oral Presentation - “Producing Bouncing Oil Droplets to Macroscopically Model Single-Particle Diffraction”.
- November, 2018. Mary Stuart Rogers Family Oral Presentation - “Producing Bouncing Oil Droplets to Macroscopically Model Single-Particle Diffraction.”
- November, 2018. Murdock College Science Research Conference Poster Presentation - “Producing Bouncing Oil Droplets to Macroscopically Model Single-Particle Diffraction.”
- December, 2018. Willamette University Research Seminar Oral Presentation - “Modeling Single-Particle Diffraction with Bouncing Droplets.”
- April, 2019. Willamette University SSRD Oral Presentation - “Bouncing Oil Droplets - A Macroscopic Model of Single-Particle Diffraction.”
- May, 2019. Willamette-Linfield-Pacific Poster Presentation - “Bouncing Oil Droplets - A Macroscopic Model of Single-Particle Diffraction.”

## Acknowledgments

I'd first like to thank my advisor, Dr. Daniel Borrero, for all of his guidance in the process of conducting this study. He was always willing and helpful in answering my many questions and troubleshooting my many lab mishaps, and taught me so much about the research process and this particular area of study. I'd also like to thank my lab assistants Tara and Tyler for all of their hard work and for being a pleasure to work alongside. Additionally, I'd like to thank Dr. Rick Watkins for lending his wizard-like data analysis skills to my study in the little spare time he had.

It wouldn't have been possible to get as far in my thesis as I did without the opportunity to begin my research last summer as part of the Science Collaborative Research Program. I would like to thank both SCRP and the Mary Stuart Rogers Foundation for funding that opportunity. I would also like to thank the Physics Department for fostering an amazing environment in which to explore physics. I've always been inspired by both my professors and fellow students and I couldn't have made it this far without them. Lastly, I'd like to thank my parents for providing me with more opportunity in life than I could ask for. They've supported me in all of my pursuits through both their ups and downs and I'm forever grateful.

# Abstract

**General Abstract:** When an oil droplet comes in contact with a vibrating oil bath it can bounce on its surface for extended periods of time. Our project aims to further investigate the similarity of bouncing droplet behavior to phenomena at the subatomic level described by quantum mechanics. We will do this by using bouncing oil droplets to experimentally model the quantum phenomenon of single-particle diffraction in which subatomic particles such as photons or electrons disperse from a slit in a pattern characteristic of waves. Our experiment will consist of directing bouncing droplets through single slit barriers of varying slit widths and measuring their angle of diffraction, i.e., how they are redirected. The purpose of this is to confirm whether or not there is a range of slit widths in which droplets create a diffraction pattern similar to subatomic particles and thus imitate this phenomenon. If so, this system could provide a way to investigate quantum mechanics on a visible scale, but our results cast doubt on this possibility.

**Technical Abstract:** When a fluid bath of oil is vertically vibrated, an incident millimetric oil droplet can bounce on its surface indefinitely and even be propelled across the surface by the waves generated by its collisions. The purpose of this project is to further investigate the extent to which the behavior of bouncing oil droplets is analogous to quantum mechanics. We will do this through experimentally modeling single-particle diffraction with bouncing oil droplets by sending them through single-slit barriers of varying slit widths and measuring the angle at which they are diffracted. Earlier studies found that the diffraction pattern of bouncing droplet closely resembled that of subatomic particles, which they attributed to the nature of bouncing droplets being analogous to the pilot wave theory of quantum mechanics. This research experimentally tests a theoretical simulation that refutes this relationship and rather concludes that their diffraction pattern is a result of their angles of diffraction being directly dependent on the droplets' impact parameter relative to the slit, i.e. the distance between the droplets' path and the centerline of the slit. The results of our study support this conclusion and cast further doubt on this system's potential to be used to further investigate the pilot wave theory of quantum mechanics on a visible scale.

# Table of Contents

<b>Acknowledgments</b>	<b>iii</b>
<b>Abstract</b>	<b>iv</b>
<b>List of Figures</b>	<b>vi</b>
<b>1 Introduction</b>	<b>1</b>
<b>2 Background</b>	<b>4</b>
2.1 Bouncing Droplet Mechanics . . . . .	4
2.2 Wave-Particle Duality . . . . .	6
2.3 The Walker System as a Quantum Analog . . . . .	7
2.4 The History of Pilot Wave Theory . . . . .	8
2.5 Past Studies . . . . .	9
<b>3 Methods</b>	<b>13</b>
3.1 Setup . . . . .	13
3.2 Materials . . . . .	13
3.3 Procedure . . . . .	17
<b>4 Results</b>	<b>21</b>
4.1 Raw Data . . . . .	21
4.2 Analysis . . . . .	22
4.3 Sources of Error . . . . .	26
4.4 Deviations from Pucci et al. Study . . . . .	27
<b>5 Conclusion</b>	<b>29</b>
5.1 Future Work . . . . .	30
<b>Bibliography</b>	<b>31</b>

## List of Figures

- |     |   |    |
|-----|---|----|
| 1.1 | The diffraction pattern of a laser emitted through a narrow slit, known as single slit diffraction. The pattern is due to the wave interference of the laser light's photons, displaying their wave-particle duality [2]. . . . .   | 1  |
| 1.2 | The figure on the left illustrates the walker angle of diffraction. On the right is the histogram of Couder and Fort's single-slit experiment with the plot of the amplitude of the interference pattern of a monochromatic wave fitted over the data, which will be explained in more depth in Chapter 2. $N$ denotes the number of droplets diffracted at a given angle [1]. . . . .  | 2  |
| 2.1 | Bouncing oil droplets on a vibrating fluid bath produced by our droplet generator. Each is surrounded by the radial Faraday waves created by their collisions with the bath surface. . . . .  | 4  |
| 2.2 | On the left is a graph of the different regimes of droplet behavior. The horizontal axis represents the driving acceleration of the bath vibration over the gravitational constant and the vertical axis represents the droplet diameter. B indicates the bouncing regime and W indicates the walker regime [7]. On the right is a picture of a fluid bath that has collapsed into a field of Faraday waves due to the driving acceleration of the vibration exceeding the Faraday threshold. . . . . | 5  |
| 2.3 | (a) Side view of the the slit structure. (b) Pucci et al.'s fluid bath setup, consisting of the droplet launcher in white and the slit structure in grey. In yellow are illustrations of parameters including the impact parameter ( $y$ ), slit width ( $L$ ), and angle of diffraction ( $\alpha$ ) [6].  | 10 |

2.4	The resulting data from Pucci et al.'s study. (a) The experimental data from their original single-slit setup with slit width $L = 3.1\lambda_F$ , and path memory $M = 0.998 \pm 0.002$ . The droplet trajectories are drawn on the left, in the middle the impact parameter over slit width is plotted against the angle of diffraction to show their relation, and a continuous probability distribution corresponding to the curve they fit to their scatter plot is plotted on the right. (b) The walker paths for all of their theoretically simulated trials in three different slit widths of $L = 4\lambda_F, 10\lambda_F$ and $20\lambda_F$ , and $M = 0.99$ above the histograms of each slit width's corresponding probability distribution [6]. . . . .	12
3.1	The complete setup of our experiment. It includes the droplet generator mounted in the top right of the image above the fluid bath and lid, which sits atop the shaker system that is mounted on the steel leveling mount. Sitting above the rest of the setup is the camera we used to film the droplets' motion. . . . .	14
3.2	The schematic of the droplet generator outlined by Harris et al. [12]. Our droplet generator follows this design exactly including all of the components shown and labeled above. . . . .	15
3.3	Our fluid bath setup without any silicone oil in it. Mounted in the bath is the 3D printed disk with the droplet launcher being the Y-shaped structure that opens toward the slit. The impact parameter of this particular setup is zero. The Plexiglas piece in the top right corner is the end of the ramp that directs the newly produced droplets onto the bath. . . . .	16
3.4	An example of an analyzed image we used to size the generated droplets. The green ring around the droplet and the red dot in the center were drawn by the Python program we used called the Hough Circle Transform. It can locate a circular shape in an image and determine its radius in pixels [13]. . . . .	18
3.5	A visual of the Tracker video analysis software we used to measure the diffraction angle of each trial. The yellow line is the walker's trajectory automatically traced out by the program frame-by-frame, the orange line is the walker's initial trajectory initialized by the droplet launcher and the blue lines are the protractor feature of the program that we aligned to measure the angle between the two trajectories [14]. . . . .	20

4.1	3D models of our fluid bath setups for $L = 4\lambda_F$ , with $y/L = 0$ (left) and $y/L = 0.4$ (right). The position of the Y-shaped droplet launcher determines the impact parameter as the walkers are sent through it to initialize their trajectories. These models were 3D printed and mounted in our fluid bath. . . . .	21
4.2	Our walker diffraction histogram from the slit width $L = 4\lambda_F$ with the Fraunhofer curve plotted over it. Visible are five pronounced peaks on the histogram that align fairly well with the peaks of the Fraunhofer curve, but are much greater in amplitude. . . . .	22
4.3	Our walker diffraction histogram from the slit width $L = 8\lambda_F$ with the Fraunhofer curve plotted over it. Visible are four sharp peaks on the histogram that align roughly with the outer peaks of the Fraunhofer curve, but are much greater in amplitude. Lacking in the histogram is the central peak present in the Fraunhofer curve. . . . .	23
4.4	Our walker diffraction histogram from the slit width $L = 8\lambda_F$ for the impact parameters $y/L = 0.2$ (left) $y/L = 0.4$ (right), both of which are reflected onto the opposite side to simulate the negative value of their respective impact parameters. Visible in each are two sharp peaks that correspond to peaks in the complete $L = 8\lambda_F$ histogram shown in Fig. 4.2. This indicates the dependence of the diffraction angle on the impact parameter is likely the cause of the peaks in our two complete histograms. . . . .	24
4.5	Our impact parameter versus diffraction angle scatter plot for the slit width $L = 4\lambda_F$ . The blue points represent individual trials while the yellow points are the average diffraction angle for each impact parameter. None of the averages varied more than $16^\circ$ from $\alpha = 0^\circ$ with no clear trend visible. . . . .	25
4.6	Our impact parameter versus diffraction angle scatter plot for the slit width $L = 8\lambda_F$ . The blue points represent individual trials while the yellow points are the average diffraction angle for each impact parameter. Its distribution is very linear and oriented down and to the right, as illustrated by the line we fit to it colored in green, indicating a negative correlation of the two variables similar to the dependence of $\alpha$ on $y/L$ found by Pucci et al., illustrated in Fig. 2.4. . . . .	25

# 1 Introduction

When people consider the limitations of the human perspective of the universe, they commonly look toward larger scales. But, in reality, some of modern science's biggest mysteries exist on smaller scales than what we can observe by eye. Quantum mechanics studies the behavior of some of the smallest particles that we know to exist, otherwise known as subatomic particles, and one phenomenon it has yet to fully explain is their wave-particle duality. This refers to the fact that, depending on the experimental conditions, these particles can be observed to behave either as a particle or as a wave. A common example of this is single particle diffraction with light particles called photons. Even though light can be detected as individual particles, if you send laser light through a slit, the resulting pattern emitted onto the screen would be the interference pattern characteristic of waves, shown in Fig. 1.1. Furthermore, if you sent one photon through the slit at a time, they would accumulate into an identical pattern. This contradictory behavior is something we have yet to understand in quantum mechanics, though there have been many theories that attempt to explain it. In 2006, Couder and Fort showed that bouncing oil droplets could provide a way for us to take a closer look at this bizarre behavior [1].

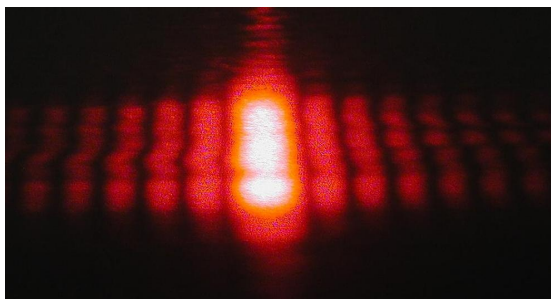


Figure 1.1: The diffraction pattern of a laser emitted through a narrow slit, known as single slit diffraction. The pattern is due to the wave interference of the laser light's photons, displaying their wave-particle duality [2].

To understand Couder and Fort’s work, consider a raindrop falling into a puddle. When the droplet collides with the fluid surface, it quickly breaks its form and merges with the rest of the fluid in the puddle. Couder and Fort discovered that if we were to recreate this situation in a lab setting with oil and vertically vibrate the fluid bath, the droplet instead bounces on the fluid surface for an extended period of time. These collisions with the fluid surface create a field of radial waves within the bath that the droplet interacts with on later collisions. This interaction can cause droplets to be propelled across the surface of the bath by their own wave fields, at which point we call them walkers. The interaction of these droplets with their surrounding wave field allows them to exhibit a sort of wave-particle duality that was originally thought to be unique to quantum mechanics [3].

In 2006, Couder and Fort provided the first evidence of this relationship by modeling single-particle diffraction with walkers. They did this by sending walkers through a slit mounted within a fluid bath and recording the angle at which they were redirected in relation to their initial trajectory, denoted as  $\alpha$  in Fig. 1.2. The cause of this redirection is due to the interaction between the slit and the wave field created by the bounces of the droplet. If the droplet’s activity was not

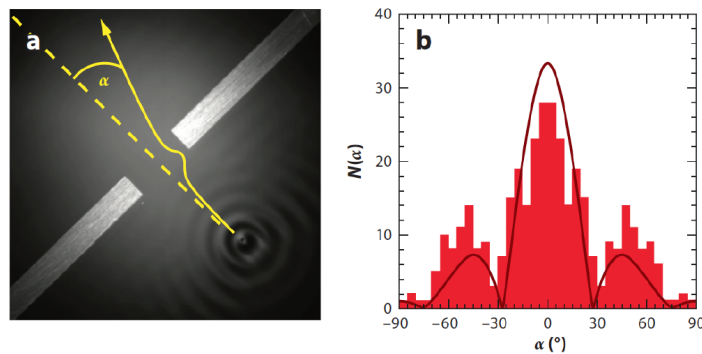


Figure 1.2: The figure on the left illustrates the walker angle of diffraction. On the right is the histogram of Couder and Fort’s single-slit experiment with the plot of the amplitude of the interference pattern of a monochromatic wave fitted over the data, which will be explained in more depth in Chapter 2.  $N$  denotes the number of droplets diffracted at a given angle [1].

associated with any wave field it would simply travel straight through the slit, but the resulting histogram in Fig. 1.2 clearly shows that this is not the case. This is due to the droplets’ waves spreading out through the slit and guiding the droplets in a variety of directions, an effect known as diffraction. Thus, the histogram serves as the diffraction pattern of these droplets. This pattern shows significant similarities to the behavior of subatomic particles, such as photons being sent through a narrow slit one at a time, which would result in the pattern introduced

in Fig. 1.1. Couder and Fort illustrated this resemblance by scaling the diffraction pattern of a plane wave to their data, shown by the curve laid over the histogram in Fig. 1.2.

To explain their results, Couder and Fort pointed to Louis de Broglie's pilot wave theory of quantum mechanics [4]. It claims that the wave-particle duality of subatomic particles is due to them having a well-defined motion that is guided by an associated wave field. This theory is strikingly similar to the nature of bouncing droplets due to their analogous droplet-wave interaction. For this reason, Couder and Fort argued that the walker system can serve as a macroscopic model of pilot wave theory that we can use to further investigate it [1]. Pilot wave theory was mostly overshadowed by the leading Copenhagen interpretation that describes subatomic particle activity in terms of probability. But many, including Einstein, believed this theory to be an incomplete description of reality [5]. As pilot wave theory provides a less ambiguous description of quantum mechanics, it has the potential to lead to a new understanding of this enigmatic area of physics [3].

In 2017, Pucci et al. decided to investigate walker diffraction in more depth by refining Couder and Fort's setup and varying additional key parameters in the system [6]. Their resulting data were far different from the diffraction pattern characteristic of waves and quantum-particles that the prior study's results resembled. Upon further analysis, they found that the distribution of the walkers seemed to be solely due to interactions with the walls of the slit rather than interactions with their wave fields. They concluded this by showing that the angle of diffraction was dependent of the droplet's proximity to either side of the slit as it approached [6]. These findings put the relation of walkers to quantum mechanics and pilot-wave theory, supported by the work Couder and Fort, into question.

One aspect within Pucci et al.'s study was theoretical simulations of widening the slit width in the single-slit system to investigate the dominance of the walker-barrier interactions that their results had suggested. This variation of the slit width resulted in similar distributions, supporting their prior results. But, as their key finding concerned the effect of the walker's interaction with the slit, providing experimental data of the effect of varying the slit width is very relevant to their study. Our experiment aims to fill this gap in Pucci et al.'s study by replicating this theoretical simulation experimentally, to further investigate the effect of varying the slit width in this system. Our data may serve to confirm Pucci et al.'s findings as well the skepticism of this system's application to quantum mechanics. Or it will refute their results, and serve to encourage further consideration of this system's potential to provide new insights in the field of quantum mechanics.

The rest of this thesis is organized as follow: Chapter 2 will discuss the necessary background in this area of study, Chapter 3 will lay out our experimental setup and methods, Chapter 4 will present the results of our experiment, and Chapter 5 will explain the conclusions and future implications of this study.

## 2 Background

This chapter will introduce the necessary background for our study, including the mechanics of bouncing droplet systems, the quantum theory that it is related to, and the past studies that we aim to follow up on.

### 2.1 Bouncing Droplet Mechanics

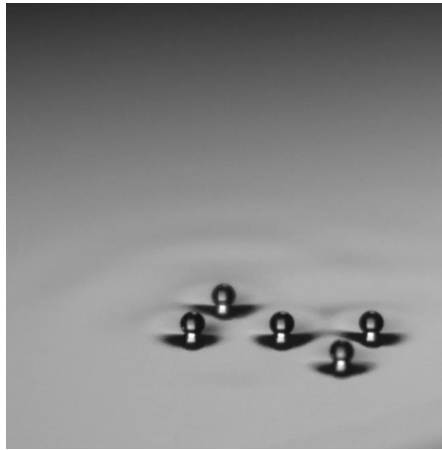


Figure 2.1: Bouncing oil droplets on a vibrating fluid bath produced by our droplet generator. Each is surrounded by the radial Faraday waves created by their collisions with the bath surface.

When a fluid droplet collides with a still fluid bath, the air layer between the two drains until it is thin enough that the attractive van der Waals force between molecules causes the droplet to break its form and merge with the bath. But, if the bath is vibrated, it can transfer enough momentum to the droplet upon collision to change its direction of motion before it merges with the bath, causing it to bounce off the surface repeatedly while maintaining its form. The merge time of the droplets depends on the density, surface tension, and viscosity of the fluid

being used. For this reason, silicone oil is commonly used in bouncing droplet experiments including ours, as it has qualities suitable for yielding this effect [3].

The vibration of the fluid bath is a key parameter in determining how these droplets will behave. It is characterized by its peak driving acceleration,

$$\gamma = A\omega^2, \quad (2.1)$$

where  $A$  is the amplitude of the vibration and  $\omega$  is its angular frequency. This driving acceleration provides the energy for the propagation of the radial waves the droplet's collisions with the bath create. The higher the driving acceleration, the longer these waves persist, up to the Faraday threshold ( $\gamma_F$ ). Above this threshold, the bath destabilizes into a field of Faraday waves, shown in Fig. 2.2. The frequencies of these waves ( $\omega_F$ ) are quantized, equal to integer multiples of half the driving frequency applied to the bath. This results in wavelengths

$$\lambda_F = 2\pi/\kappa_F \quad (2.2)$$

where  $\kappa_F$  is the Faraday wave number. In systems relevant to our experiment, the Faraday wave number can be calculated by the deep-water capillary dispersion relation

$$\omega_F^2 = \sigma\kappa_F^3/\rho, \quad (2.3)$$

where  $\sigma$  is the surface tension of the fluid and  $\rho$  is its density [3].

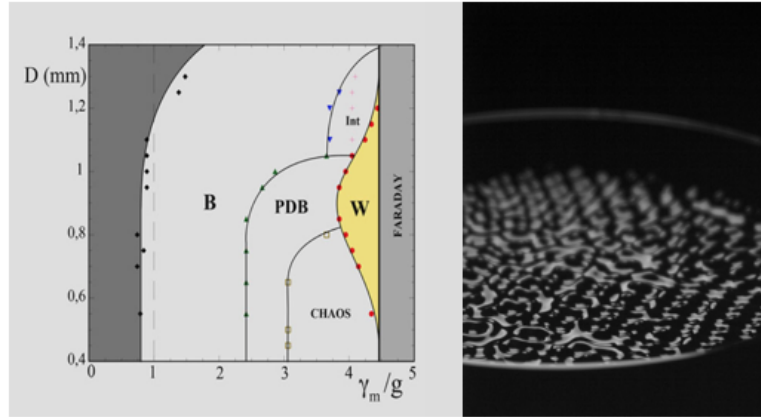


Figure 2.2: On the left is a graph of the different regimes of droplet behavior. The horizontal axis represents the driving acceleration of the bath vibration over the gravitational constant and the vertical axis represents the droplet diameter. B indicates the bouncing regime and W indicates the walker regime [7]. On the right is a picture of a fluid bath that has collapsed into a field of Faraday waves due to the driving acceleration of the vibration exceeding the Faraday threshold.

As the driving acceleration of the vibration approaches this threshold, the radial waves created by a droplet propagate long enough for it to interact with

them on later collisions with the bath. This effect is known as the droplet's path memory [8], which Pucci et al. [6] quantified by the expression

$$M = \frac{\gamma}{\gamma_F}. \quad (2.4)$$

Thus, the closer  $\gamma$  is to  $\gamma_F$ , the closer  $M$  is to 1. Higher path memories correspond to the collision waves of the droplet sustaining longer in the bath and therefore affecting the droplet's motion on a greater number of future collisions with the bath, hence the name path memory. Small variations of the path memory can have substantial effects on the behavior of the droplet.

There exists another threshold just below the Faraday threshold known as the walker threshold. Between these two thresholds lies the walking regime colored in yellow in Fig. 2.2. In this regime, the droplet will interact with its waves in a way that propels it across the surface at a constant velocity. This regime corresponds with path memories of  $M \geq .94$ , with quantum-like behavior arising at  $M \geq .97$  [9]. Walking occurs by the droplet landing on the slope of its most recently created wave which displaces it, causing it to land on the slope of its newly created wave, further displacing it, and so on. These droplets are referred to as walkers and their interactions with their own wave field cause them to exhibit behavior with intriguing similarities to quantum mechanics [3].

## 2.2 Wave-Particle Duality

Quantum mechanics studies the behavior of subatomic particles. Before we discuss the relation of walkers to quantum mechanics, we will first explain the basic concept of wave-particle duality that is observed with subatomic particles. Understanding this phenomenon remains one of the major problems in the field of quantum mechanics today. A common example of it is the nature of light, which is made up of individual particles called photons. This could be demonstrated by shooting one photon worth of light out of a light bulb surrounded by photon detectors. If this tiny amount of light was visible to our eyes, we would see it spread out in all directions, and yet, only one photon would be detected at one specific point. This implies that light behaves like particles at the subatomic scale. Therefore, if you were to shoot a laser beam of light through a narrow slit, you would expect it to be emitted at one focused spot on the surface behind, as the particles that passed through the slit would travel straight toward the surface. Instead, the actual result of performing this experiment is the pattern shown in Fig. 1.1. The reason the pattern is spread out over the surface is an effect called diffraction in which waves spread out after propagating through a spatially confining structure which is why we refer to this as a diffraction pattern [2].

The reason for the alternation between bright and dark spots in light’s diffraction pattern is due to interference that is also characteristic of waves. A way of understanding this idea is imagining that the light exiting the slit as being made up of individual radial wave sources lined up along the length of the slit. As lasers emit monochromatic light, meaning it is of one specified wavelength, all of these radial waves possess this same wavelength. But, depending on the distance each wave travels from the slit to reach a certain point on the screen, they may either constructively or destructively interfere with one another, meaning that their amplitudes either combine or cancel out depending on if they are in phase or not [2]. For any monochromatic wave of intensity  $I_0$  and wavelength  $\lambda$  incident with a slit of width  $L$ , a function can be derived that is dependent on the angle  $\alpha$  between the slit’s centerline and the path to a given point to determine the wave’s intensity at that point. The resulting function is

$$I(\alpha) = I_0 \left( \frac{\sin(\pi L \sin \alpha / \lambda)}{\pi L \sin \alpha / \lambda} \right)^2. \quad (2.5)$$

The diffraction this function describes is known as Fraunhofer diffraction [10] and also describes the intensity of monochromatic light’s diffraction pattern, providing evidence that light exhibits wave behavior in addition to particle behavior, a duality that has yet to be fully understood [6].

## 2.3 The Walker System as a Quantum Analog

This concept of wave-particle duality is what ties the walker system to quantum mechanics. As walkers behave both as particles with a definite position but are also affected a surrounding wave field, they have been shown to exhibit unusual behavior analogous to many quantum phenomena including single particle diffraction, tunneling, and spin states among others [3]. The nature of bouncing droplets is especially similar to a certain theory of quantum mechanics known as pilot wave theory, which describes subatomic particles as having a definite position and trajectory determined by their surrounding wave field [11]. This idea was conceived by Louis de Broglie in the 1920s. His original conception is referred to as the “double-solution,” claiming that the particle’s behavior is determined both by a pilot wave centered on the particle as well as a statistical wave described by Schrodinger’s equation. He claims the pilot wave is linearly related to the statistical wave and originates from the particle’s internal oscillations, keeping the particle and pilot wave in resonance [3]. He relates the particle’s momentum  $p$  to its wave field with the equation,

$$p = \hbar \nabla \phi, \quad (2.6)$$

where  $\phi$  is the phase of the wave function. This relationship illustrates that the motion of the particle is directed by its wave field, hence the name pilot wave theory [11].

The walker system bears similarity to pilot wave theory that may allow walkers to effectively serve as a macroscopic model for it. This similarity includes the fact that the walker is guided by a pilot wave that is resonant with its oscillation, the pilot wave being the radial Faraday waves created by its collisions with the bath. The other key similarity is the fact that it is related to a statistical wave of the same wavelength as the pilot wave, according to the results of Couder and Fort's walker diffraction experiment that showed that walker diffraction closely resembled the amplitude of a monochromatic wave of similar wavelength to the Faraday wavelength of their system [1]. Thus, this system may allow us to investigate the nature of this theory of quantum mechanics empirically using a macroscopic system, something that is not possible with other theories of quantum mechanics [3].

## 2.4 The History of Pilot Wave Theory

Quantum mechanics contains many competing theories that aim to explain this dual behavior of subatomic particles. The leading theory today is known as the Copenhagen interpretation. Its explanation of wave-particle duality is called complementarity, which claims that subatomic particles are capable of behaving as either a particle or a wave, depending on the situation [5]. For example, when diffracting a single photon, its behavior can be described by a wave function with an intensity that represents the probability of finding the particle at a given point. But once we actually measure its location, that function collapses and the photon is described purely as a particle with a definite position. This theory also includes the central Heisenberg uncertainty principle that states the more you know about a particle's position, the less you can know about its momentum and vice versa. This means that once we measure the particle's position we are limited from having a complete understanding of its momentum. Even though this theory provides no qualitative understanding of quantum reality, its development gave us the ability to describe and predict subatomic particle behavior mathematically, leading to its wide acceptance [11].

When this approach was being developed in the first half of the 20th century, physicists including Einstein, Schrodinger, and De Broglie were reluctant to accept it, as they believed that reality cannot be fully described in terms of probability. They felt it neglected the idea of an independent reality at the subatomic level in which a particle has a definite trajectory [5]. For this reason, De Broglie designed his own theory of quantum mechanics that he believed could lead to further insight into reality at the subatomic level. The result was pilot wave theory [11].

While pilot wave theory could provide predictions similar to those of the Copenhagen interpretation, it could not match the leading theory's amount of support and development. This was exposed when it was presented at the 1927 Solvay Conference. Pauli pointed out its inconsistency with special relativity, specifically in the two-body scattering process, and De Broglie could not provide a convincing response. Even Einstein, who supported the idea of an alternative theory of quantum mechanics, did not come to his aid. Thus, the theory lost its credibility from then on, and remained mostly underdeveloped until Bohm further developed the theory to resolve these objections in 1952. Bohm's work even inspired De Broglie to continue developing the theory himself. Despite this, the theory never gained substantial acceptance [11].

## 2.5 Past Studies

Couder and Fort investigated the novel relationship between the bouncing droplet system and quantum mechanics by performing walker diffraction. They did this by using a square fluid bath with two barriers mounted just below its surface, spaced a width  $L$  apart to form a slit. They sent 125 walkers through a slit of width  $L = 14.7$  mm such that  $L/\lambda_F = 2.11$ . The resulting diffraction pattern is shown in Fig. 1.2. The curve they fit over it is the amplitude of Fraunhofer diffraction, expressed by the function

$$A(\alpha) = A_0 \left| \frac{\sin(\pi L \sin \alpha / \lambda)}{\pi L \sin \alpha / \lambda} \right|, \quad (2.7)$$

with  $A_0$  being the initial amplitude of the monochromatic wave incident on the slit. This is related to but different from the intensity of Fraunhofer diffraction expressed in Eq. 2.5, as it gives the wave's amplitude rather than its intensity. They also performed this procedure in a system of two slits, as well, to replicate Young's double-slit experiment, which also resulted in a diffraction pattern resembling the amplitude of the Fraunhofer diffraction of a monochromatic wave incident on two slits [1].

In their study, Couder and Fort acknowledge some significant differences between this system and quantum mechanics that imply that its application to understanding quantum mechanics is limited. These include the fact that it occurs on a macroscopic scale, has no relation to the Planck's constant which is central to quantum theory, and that the wave field is 2D and emitted by the droplet. They also recognized that external forcing sustains the system and fixes the wavelength of the wave field, the fact that we can observe the entire trajectory of the droplet, and the fact that the diffraction pattern resembled the amplitude of Fraunhofer diffraction rather than its intensity. But, they still concluded that this system

aligns with a viable theory of quantum mechanics in De Broglie’s pilot-wave theory. Thus, these results suggest that it has similarities to the quantum realm that are worth examining further [1].

Pucci et al. recognized some shortcomings in Couder and Fort’s study that they aimed to address with an in-depth experimental and theoretical study in 2017 [6]. The flaw that Pucci et al.’s refined setup addressed first and foremost was Couder and Fort’s lack of reporting key parameters in their setup. These included the droplet size they used in their system as well as the forcing amplitude of their vibration, both of which have been found to have a significant influence on how the droplet will behave. They also refined their setup by using a piezoelectric droplet

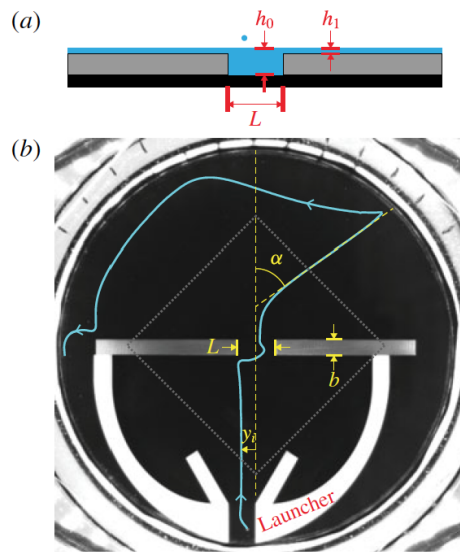


Figure 2.3: (a) Side view of the the slit structure. (b) Pucci et al.’s fluid bath setup, consisting of the droplet launcher in white and the slit structure in grey. In yellow are illustrations of parameters including the impact parameter ( $y$ ), slit width ( $L$ ), and angle of diffraction ( $\alpha$ ) [6].

generator that enabled them to manipulate the droplet size with precision, as well as a precision driver that creates a spatially uniform vertical vibration. They utilized a circular fluid bath with a similar slit structure to Couder and Fort’s. Components they added to the fluid bath included a droplet launcher structure they used to set the droplet’s initial trajectory pictured in Fig. 2.3, something that Couder and Fort provided no method for. Lastly, they added a transparent lid to protect the system from ambient air currents, which they demonstrated had a substantial effect through trials with and without the lid [6].

There were two main conclusions of Couder and Fort that Pucci et al.’s results challenged. One was the fact that their walker diffraction pattern roughly corre-

sponded to the amplitude of the Fraunhofer diffraction of a monochromatic wave incident with the slit (Eq. 2.7). The other was that the angle of diffraction  $\alpha$  is independent of the impact parameter  $y$ , which is the distance from the droplet's initial trajectory to the centerline of the slit, both illustrated in Fig. 2.3. Instead, Pucci et al.'s experimental results in the single slit system led to the following conclusions: the diffraction pattern shows no resemblance to the amplitude of the Fraunhofer diffraction of a monochromatic wave incident with a single slit, and that there exists a clear dependence of the angle of diffraction on the impact parameter of the slit. These results are illustrated in Fig. 2.4. As Pucci et al.'s study consisted of a refined setup in relation to Couder and Fort's, these results cast significant doubt on the results of the prior study. But, while their study was relatively comprehensive, they do acknowledge that there is much parameter space that has yet to be explored in this system that could still yield Fraunhofer diffraction of walking droplets [6].

Our experiment serves to further explore the effect of the slit width on the relationship between the walker's angle of diffraction and its impact parameter with the slit. Pucci et al.'s exploration of this parameter was performed only with theoretical simulations that resulted in the same dependence they found in the original setup (Fig. 2.4). For this reason, we felt an experimental replication of their theoretical simulation is necessary to exhaust this parameter's potential influence on this system that could give it a stronger relation to quantum mechanics than their study concluded. Thus, our study experimentally investigated this dependence, as well as any resemblance to Fraunhofer diffraction, in walker systems of varying slit widths.

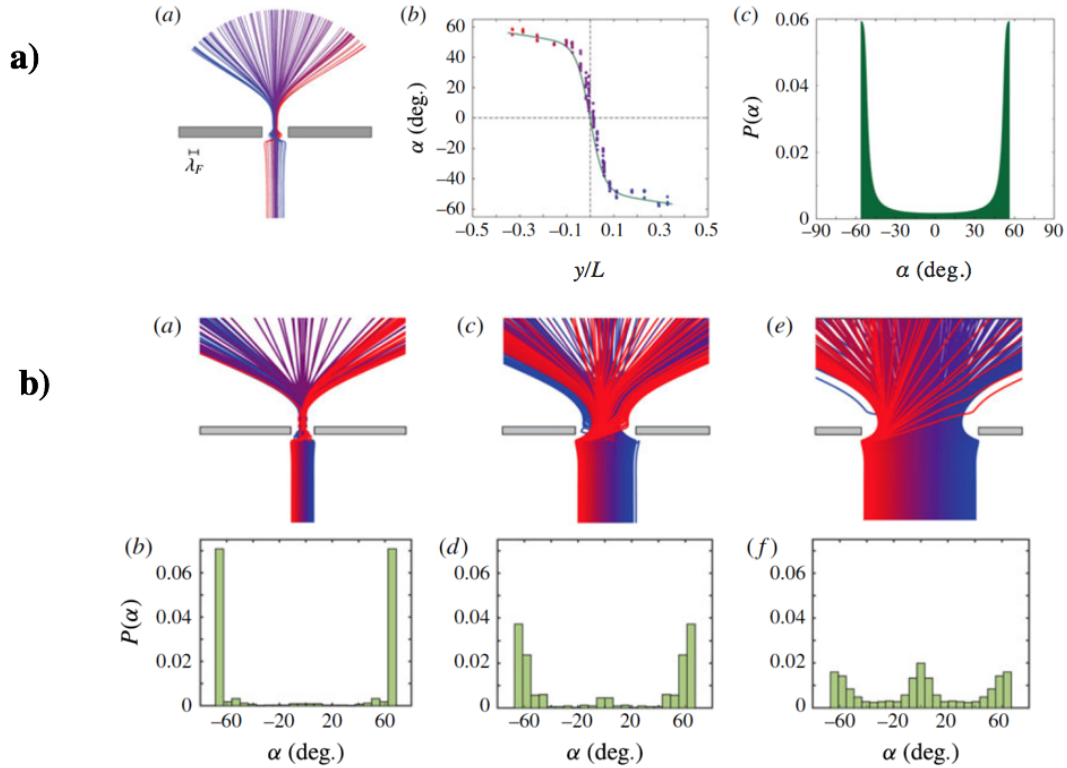


Figure 2.4: The resulting data from Pucci et al.'s study. (a) The experimental data from their original single-slit setup with slit width  $L = 3.1\lambda_F$ , and path memory  $M = 0.998 \pm 0.002$ . The droplet trajectories are drawn on the left, in the middle the impact parameter over slit width is plotted against the angle of diffraction to show their relation, and a continuous probability distribution corresponding to the curve they fit to their scatter plot is plotted on the right. (b) The walker paths for all of their theoretically simulated trials in three different slit widths of  $L = 4\lambda_F, 10\lambda_F$  and  $20\lambda_F$ , and  $M = 0.99$  above the histograms of each slit width's corresponding probability distribution [6].

## 3 Methods

In this section, we will introduce the experimental setup and procedure of our study. It is primarily based on previous studies, mainly that of Pucci et al. [6]. This is to ensure that we can achieve this droplet behavior as efficiently and consistently as possible, as well as investigate it under conditions that align with Pucci et al.'s as closely as possible, as their study is the one we aim to address.

### 3.1 Setup

Our setup, pictured in Fig. 3.1, consists of a droplet generator that sits above the fluid bath. The bath sits on top of the shaker system that provides the vertical vibration to the bath. The driving acceleration of this vibration is adjusted with a function generator that sends a signal through an amplifier to the shaker system. On top of the shaker system is an accelerometer to measure the direction and magnitude of the driving acceleration. The shaker system is mounted on a steel leveling mount. Above the fluid bath is a camera used to film the motion of the droplets within the bath.

### 3.2 Materials

This section will describe the materials used to create the setup described above.

#### 3.2.1 Silicone Oil

The silicone oil we used is Esco E200 Silicone Fluid. It has a viscosity of 20 cSt, the same as that used by Pucci et al. This has been found to have the ideal properties for bouncing droplet experiments as it can yield them in a wider parameter space than other oils that have been used. It also has a low vapor pressure to prevent it from evaporating and changing the level of the fluid bath [9].

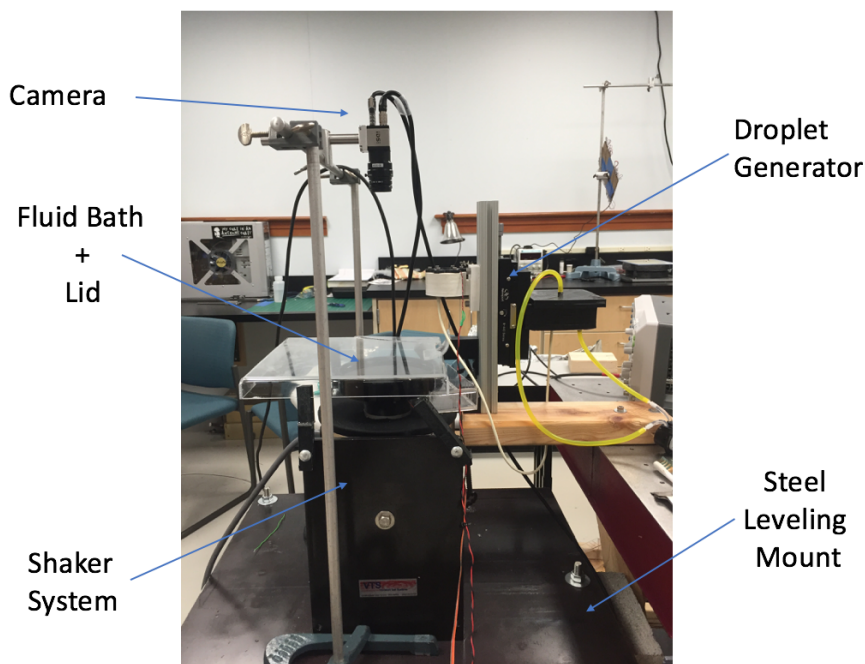


Figure 3.1: The complete setup of our experiment. It includes the droplet generator mounted in the top right of the image above the fluid bath and lid, which sits atop the shaker system that is mounted on the steel leveling mount. Sitting above the rest of the setup is the camera we used to film the droplets' motion.

### 3.2.2 Droplet Generator

Our droplet generator is based on the design by Harris et al. pictured in Fig. 3.2 [12]. Its components include a fluid reservoir mounted on a translation stage, attached to a pump, and a droplet chamber with a nozzle on bottom and a piezoelectric disk on top that is operated by a circuit with an Arduino controller board. This all sits above an oil-coated Plexiglas ramp that redirects the droplets produced to skip onto the bath without breaking the surface.

The droplets are produced from the nozzle of the droplet chamber when a signal is sent to the piezoelectric disk with the Arduino controller board, prompting it to apply a downward force to the fluid in the chamber. The length of this pulse can be adjusted with the code programmed into the Arduino board which determines how the droplet is formed. The width of the nozzle opening also plays a role in the characteristics of the produced droplet, specifically its size.

The fluid reservoir acts as a source of oil to keep the droplet chamber full at all times. It also allows us to vary the pressure applied to the nozzle tip by adjusting its height in relation to the droplet chamber with the translation stage. This is necessary to ensure that the droplets are well-formed. Too little pressure can

result in no droplet being produced, and too much pressure can lead to multiple droplets being produced. The pump allows the level of the fluid reservoir to be consistent by pumping oil into the center pool, overflowing it into a surrounding pool that runs back into the pump.

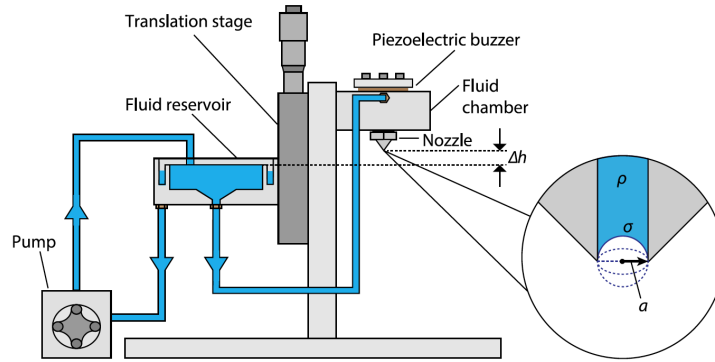


Figure 3.2: The schematic of the droplet generator outlined by Harris et al. [12]. Our droplet generator follows this design exactly including all of the components shown and labeled above.

### 3.2.3 Fluid Bath

The fluid bath was machined out of anodized aluminum. It is circular with a diameter of 13.3 cm. This is slightly smaller than the 16 cm diameter bath used by Pucci et al., but it was what we had available and we felt it would serve our purposes well enough. Inside the bath we mounted a 3D printed disk that is 1 mm thick and has the slits and droplet launcher attached to it, pictured in Fig. 3.3. We mounted it using flowable silicone glue. In order to vary the position of the droplet launcher and the width of the slit, we reprinted this disk with the desired parameters to remount in the bath. To protect the bath from ambient air currents we use a clear Plexiglas lid mounted to the shaker system with 3D printed supports.



Figure 3.3: Our fluid bath setup without any silicone oil in it. Mounted in the bath is the 3D printed disk with the droplet launcher being the Y-shaped structure that opens toward the slit. The impact parameter of this particular setup is zero. The Plexiglas piece in the top right corner is the end of the ramp that directs the newly produced droplets onto the bath.

### 3.2.4 Shaker System and Leveling Mount

Our shaker system was manufactured by Vibration Test Systems (model VG-80 CA-6). It has a rated force of 80 lbf meaning it is easily capable of vibrating our fluid bath with a consistent driving acceleration as it takes approximately half of that value to vibrate our bath at the driving acceleration we require. It has a useful frequency range of 2-10000 Hz, and a dynamic stroke of 0.75", which allows it to produce the desired amplitude and frequency of vibration.

We machined the leveling mount from an 2'  $\times$  2'  $\times$  1" steel plate. We drilled three holes into it that we put the leveling legs into, allowing us to easily level the fluid bath using a bubble level. In order to bring the fluid bath closer to the level of the droplet generator mounted on a table, we stacked the leveling mount on top of cinder blocks.

### 3.2.5 Function Generator, Amplifier and Oscilloscope

The function generator we used was a Tektronix CFG 253 3MHz Function Generator, which was capable of providing the needed 80 Hz oscillation frequency to the shaker system. This was amplified using a Crown 2002 Xti Series audio amplifier that amplified the signal of the function generator into the voltage range

required by the shaker system. We used a RIGOL DS1054Z digital oscilloscope in order to more accurately measure the frequency of the wave function created by our function generator that was sent to the shaker system, as well as measure the amplitude of the driving acceleration of the fluid bath measured by our accelerometer.

### 3.2.6 Accelerometer

The accelerometer we used to measure the driving acceleration of the bath was an Adafruit ADXL326 triple-axis accelerometer. This was mounted directly below the center of the oil bath. We wired it to the oscilloscope in order to measure its oscillation. We were only interested in the vertical acceleration of the bath so we wired only the z-axis output to send a signal to the oscilloscope.

### 3.2.7 Camera

The camera we used to film the motion of the droplets was an IDS UI-3140CP-M-GL Rev. 2 with a Navitar MVL 12M23 lens. This setup had the needed magnification, resolution and shutter speed needed to yield videos in which the droplets could be accurately tracked using tracking software. We positioned it to have a bird's-eye view of the bath exactly in the center of it. This was important to ensure that our measured angles of diffraction were accurate.

### 3.2.8 3D Printer

The 3D printer we used was a LulzBot Taz 6. We used it with HIPS and ABS filaments. We used it to print the fluid bath and droplet chamber of the droplet generator, the slit and droplet launcher setups that we mounted into the fluid bath, as well as the supports for the transparent fluid bath lid. We sealed the parts that hold fluid with 3D print coating to avoid leaks. Before using this method, we experimented with sealing parts with acetone vapor baths, which is why we switched between filament types.

## 3.3 Procedure

We first had to locate the walking regime by adjusting different parameters of the bath vibration. Once we had done that we were ready to begin sending the walkers through the slit system and measuring their angles of diffraction. This process is outlined in the following section.

### 3.3.1 Creating Walkers

Locating the walking regime shown in Fig. 2.2 requires controlling the droplet diameter, as well as the driving acceleration that depends on the driving frequency and amplitude expressed in Eq. 2.1.

We set the droplet diameter to  $0.69 \pm 0.04$  mm by varying the nozzle diameter of the droplet generator. Pucci et al.'s study used a droplet diameter of 0.67 mm. We checked magnitude and consistency of the droplet diameter by producing 100 droplets in a row and capturing images of each of them. We then processed those images with a Python program that returned the diameters in pixels [13] which we could then convert to mm by using a resolution target as a reference. In the images we analyzed, we found that every droplet was either 24 or 25 pixels in diameter. This one pixel in variance corresponded to an error of 0.04 mm.

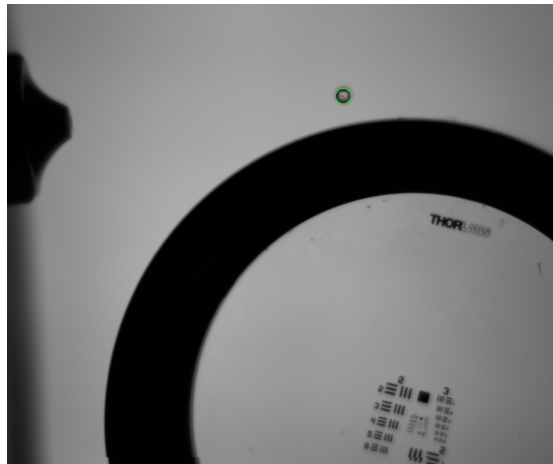


Figure 3.4: An example of an analyzed image we used to size the generated droplets. The green ring around the droplet and the red dot in the center were drawn by the Python program we used called the Hough Circle Transform. It can locate a circular shape in an image and determine its radius in pixels [13].

The driving frequency was set to 80 Hz, which was also specified in Pucci et al.'s study. We then set the amplitude above the Faraday threshold and slowly decreased it until no standing Faraday waves were visible. The resulting path memory measurement was  $M = 0.97 \pm 0.03$  as compared to  $M = 0.99$  used in Pucci et al.'s theoretical simulation.

### 3.3.2 Varying the Slit Width

The theoretical simulation of varying the slit width in Pucci et al.'s study, illustrated in Fig. 2.4, included slit widths of  $L = 4\lambda_F, 10\lambda_F$  and  $20\lambda_F$  with  $\lambda_F$

determined by Eq. 2.3. We use the same fluid with the same viscosity and surface tension as well as the same bath depth as their study. As the Faraday wavelength is only dependent on those variables, ours has the same value which they calculated to be 4.75 mm. They started with  $4\lambda_F$  because they found in their experimental work that slit widths less than that led to the dependence of the angle of diffraction on the impact parameter. Our study includes slit widths of  $4\lambda_F$  and  $8\lambda_F$ . This is because  $20\lambda_F$  would be too wide for the size of our fluid bath.

### 3.3.3 Varying the Impact Parameter

We tested impact parameters of  $y/L = 0.4, 0.2$  and  $0$ , all being on the left side of the slit. This will evenly cover a half of the width of the slit. While Pucci et al.'s simulation varied the impact parameter over the entire width of the slit, the symmetry of the slit allowed us to only vary it over one half of the slit width and reflect that data onto the other side to effectively cover the whole slit width.

### 3.3.4 Walker Diffraction

To diffract a walker, we generated a droplet that was directed into the open half of the bath. We would then direct the droplet into the path along the border of the bath created by the droplet launcher shown in Fig. 3.3 by blowing on it to alter its path. The disturbance this caused to the bath surface was quickly damped out, well before the droplet was diffracted. The launcher then directed the droplet to be launched toward the slit at a given impact parameter.

### 3.3.5 Video Analysis

This walker's path was recorded by the camera above, a video that we would then analyze with Tracker video analysis software to determine at what angle it was diffracted by the slit as shown in Fig. 3.5 [14]. This software works by locating a specified object within each successive frame of a video and then piecing those positions together into a continuous path. It also has measurement tools including a protractor that allowed us to determine the angle between the initial and final path of the droplet, which we refer to as the angle of diffraction.

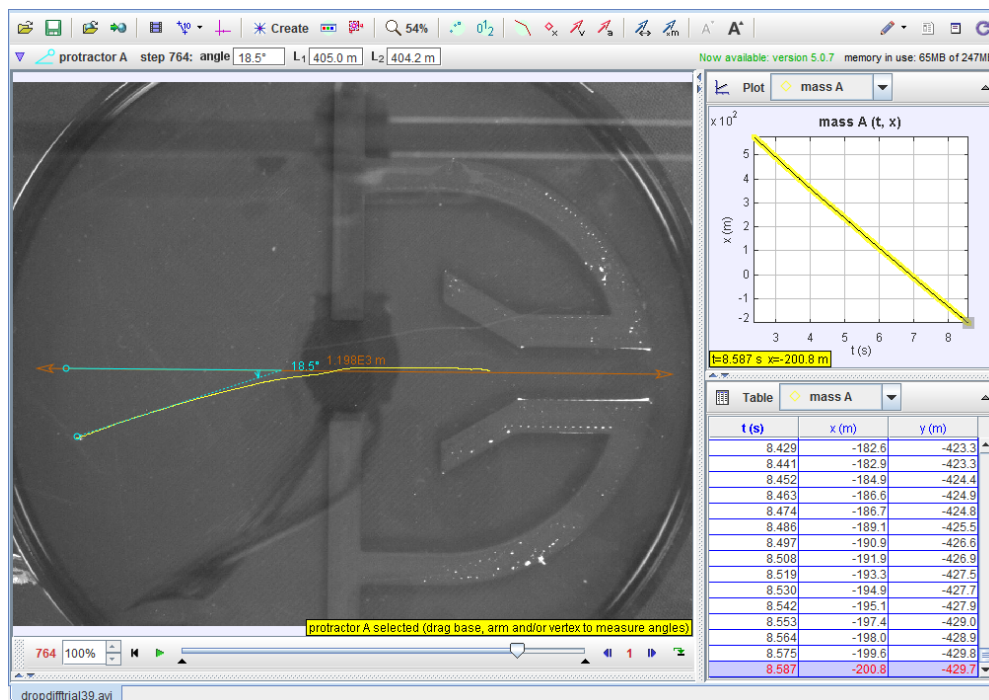


Figure 3.5: A visual of the Tracker video analysis software we used to measure the diffraction angle of each trial. The yellow line is the walker's trajectory automatically traced out by the program frame-by-frame, the orange line is the walker's initial trajectory initialized by the droplet launcher and the blue lines are the protractor feature of the program that we aligned to measure the angle between the two trajectories [14].

## 4 Results

In this chapter, I will present the raw data we collected and the results they yielded upon analysis. Additionally, I will outline all sources of error in our system as well as deviations from the setup of Pucci et al.

### 4.1 Raw Data

Our raw data consisted of 297 individual videos of a droplet being diffracted through a single slit structure. The two manipulated variables were impact parameter and slit width. We included two slit widths of  $4\lambda_F$  and  $8\lambda_F$ , and three impact parameters of  $0L$ ,  $0.2L$  and  $0.4L$  for each of those widths, resulting in a total of six slit structures (Fig. 4.1). We ran approximately 50 trials within each structure.

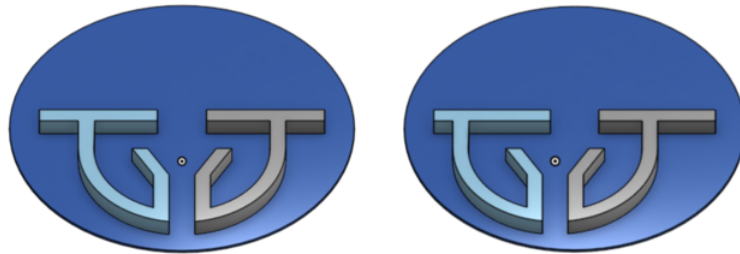


Figure 4.1: 3D models of our fluid bath setups for  $L = 4\lambda_F$ , with  $y/L = 0$  (left) and  $y/L = 0.4$  (right). The position of the Y-shaped droplet launcher determines the impact parameter as the walkers are sent through it to initialize their trajectories. These models were 3D printed and mounted in our fluid bath.

The videos were analyzed with Tracker, a video analysis software [14]. After manually identifying the droplet in a given frame, the droplet's path was drawn out by the program. We would then use a protractor feature within the program

to measure the angle between the droplet’s initial path and its final path. Thus, our raw data resulted in 297 measured angles, each corresponding to a specific slit width and impact parameter.

## 4.2 Analysis

The purpose of this study was to either confirm or refute two of Pucci et al.’s key findings from their theoretical manipulation of the slit width. These were that, in the tested slit widths, the droplets’ diffraction patterns do not resemble Fraunhofer diffraction and that there is a clear dependence of the diffraction angle on the impact parameter.

In order to address the first conclusion of Pucci et al., we made diffraction patterns of the walkers diffracted from each slit width. We did this by compiling the 149 diffraction angles measured in the  $L = 4\lambda_F$  slit width onto one histogram and the 148 measured in the  $L = 8\lambda_F$  slit width onto another. We wanted these diffraction patterns to span the entire slit width rather than just the half that we ran trials on so we reflected our data from  $y/L = 0.2$  and  $0.4$  onto the other half of the slit, which was valid due to the symmetry of the slit. This resulted in 248 data points in the  $L = 4\lambda_F$  histogram (Fig. 4.2) and 247 in the  $L = 8\lambda_F$  histogram (Fig. 4.3). We adjusted the number of bins to make the curve of each histogram appear as continuous as possible. To compare them to Fraunhofer diffraction we plotted Eq. 2.7 over each with the corresponding variable values. This allowed us to easily discern any significant similarity between the two diffraction patterns.

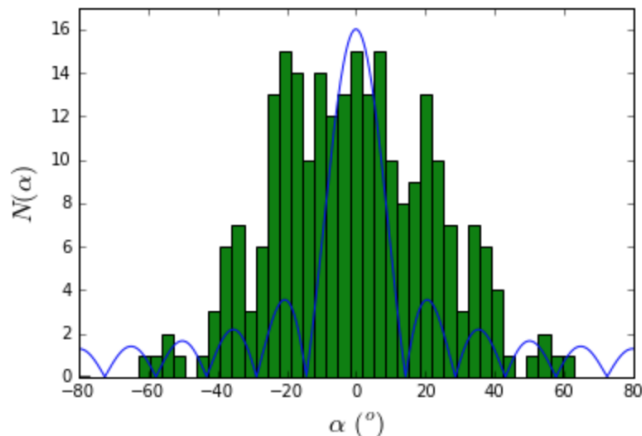


Figure 4.2: Our walker diffraction histogram from the slit width  $L = 4\lambda_F$  with the Fraunhofer curve plotted over it. Visible are five pronounced peaks on the histogram that align fairly well with the peaks of the Fraunhofer curve, but are much greater in amplitude.

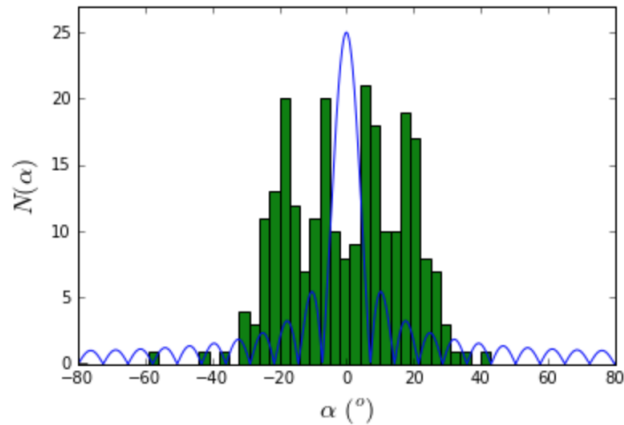


Figure 4.3: Our walker diffraction histogram from the slit width  $L = 8\lambda_F$  with the Fraunhofer curve plotted over it. Visible are four sharp peaks on the histogram that align roughly with the outer peaks of the Fraunhofer curve, but are much greater in amplitude. Lacking in the histogram is the central peak present in the Fraunhofer curve.

The  $4\lambda_F$  slit width yielded a somewhat bell-shaped histogram with five pronounced peaks. Laying the Fraunhofer curve over it showed significant alignment between the peaks of the two diffraction patterns. The main difference was that the peaks of the histogram were much greater in amplitude than those of the Fraunhofer curve to either side of the central peak. The  $8\lambda_F$  slit width's histogram was more concentrated around zero, a trend found by Pucci et al. for wider slit widths. There were four sharp peaks, two to either side of  $\alpha = 0^\circ$  that partially aligned with the two peaks to either side of the center peak of the Fraunhofer curve. Like the other histogram, their amplitudes were far greater than those of the Fraunhofer peaks they aligned with. It was also missing the central peak present on the Fraunhofer curve.

We also observed that there are the same number of peaks as there are impact parameters in our data, at least in the smaller slit width, indicating the peaks may be a result of the impact parameter manipulation yielding points concentrated at certain diffraction angles. We confirmed this by creating histograms for each impact parameter, like the one shown in Fig. 4.4, and found that they had defined peaks that corresponded to peaks in the complete histograms. The  $8\lambda_F$  slit width had exactly one peak for each impact parameter, indicating the diffraction angle is dependent on the impact parameter, as found by Pucci et al. It is missing a peak corresponding to the  $y/L = 0$  impact parameter, but upon further analysis we found that this peak was wider and contributed to the peaks to either side of  $\alpha = 0^\circ$ , making it invisible in the complete histogram. There were multiple peaks for each impact parameter in the  $4\lambda_F$  slit width but we attributed this to

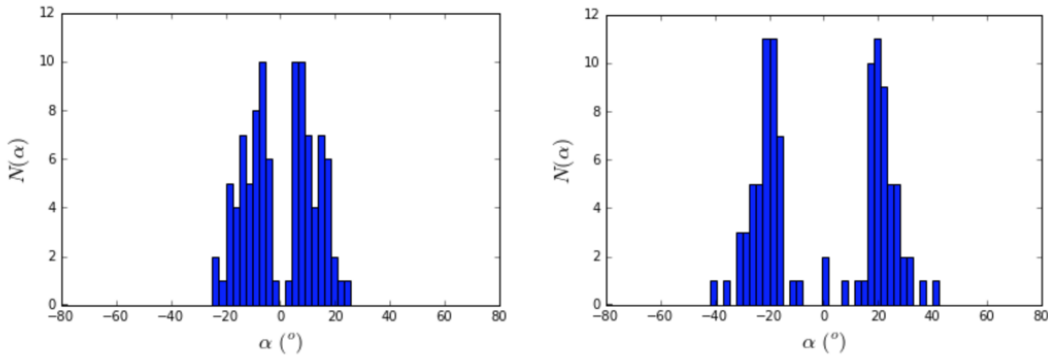


Figure 4.4: Our walker diffraction histogram from the slit width  $L = 8\lambda_F$  for the impact parameters  $y/L = 0.2$  (left)  $y/L = 0.4$  (right), both of which are reflected onto the opposite side to simulate the negative value of their respective impact parameters. Visible in each are two sharp peaks that correspond to peaks in the complete  $L = 8\lambda_F$  histogram shown in Fig. 4.2. This indicates the dependence of the diffraction angle on the impact parameter is likely the cause of the peaks in our two complete histograms.

the fact that varying the impact parameter in a smaller slit width leaves a smaller margin for error as our impact parameter was quantified as a fraction of the total slit width. Therefore, our manipulation of it may have been less accurate in that slit width, causing more than one concentration of diffraction angles within each setup.

We addressed the second finding of Pucci et al. by creating a scatter plot of  $y/L$  versus  $\alpha$  for each slit width shown in Figs. 4.5 and 4.6. Each consisted of the same data points that we used to create the histograms. These were then analyzed for any visible trends similar to that found in Pucci et al.'s data shown in Fig. 2.4, which they fit with a curve to illustrate. In order to better discern any general trends, we took the average diffraction angle at each impact parameter which we plotted in yellow over the rest of the individual data points.

The  $L = 4\lambda_F$  scatter plot had a wide spread of diffraction angles for each impact parameter, each with a range of at least 60 degrees. Taking each of their averages showed that all five impact parameters had an average diffraction angle no further than 16 degrees from zero. Thus, no significant trend could be drawn from this, let alone one that remotely resembled that found by Pucci et al. (Fig. 2.4). The  $L = 8\lambda_F$  scatter plot had more concentrated distributions of  $\alpha$  for each value of  $y/L$ . This allowed for a visible trend that was very linear and negatively oriented down and to the right, indicating a dependence of  $\alpha$  on  $y/L$ . This matched the negative orientation of the trend of Pucci et al.'s, but differed in that it was a linear rather than the exponential relationship shown by the curve

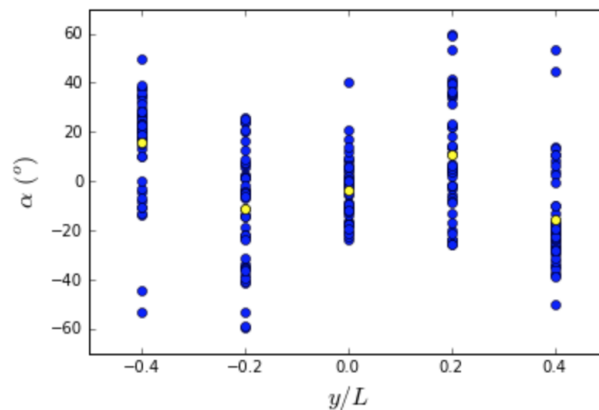


Figure 4.5: Our impact parameter versus diffraction angle scatter plot for the slit width  $L = 4\lambda_F$ . The blue points represent individual trials while the yellow points are the average diffraction angle for each impact parameter. None of the averages varied more than  $16^\circ$  from  $\alpha = 0^\circ$  with no clear trend visible.

they fit to their scatter plot.

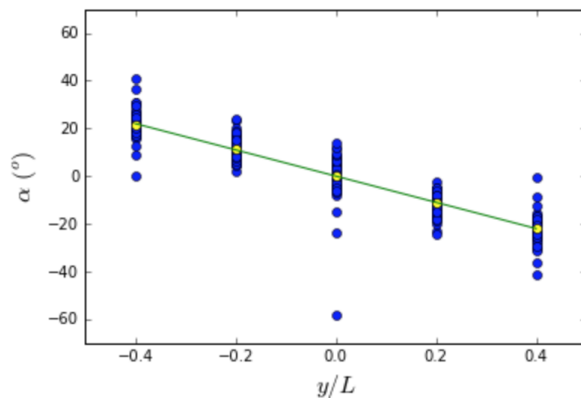


Figure 4.6: Our impact parameter versus diffraction angle scatter plot for the slit width  $L = 8\lambda_F$ . The blue points represent individual trials while the yellow points are the average diffraction angle for each impact parameter. Its distribution is very linear and oriented down and to the right, as illustrated by the line we fit to it colored in green, indicating a negative correlation of the two variables similar to the dependence of  $\alpha$  on  $y/L$  found by Pucci et al., illustrated in Fig. 2.4.

## 4.3 Sources of Error

The system in which we performed our study is affected by many different parameters making it important to acknowledge the sources of error that are associated with them. These are outlined in this section.

### 4.3.1 Impact Parameter

We varied our impact parameter between trials by re-positioning the Y-shaped droplet launcher in our bath setup as illustrated in Fig. 4.1. While, in theory, this was an exact manipulation of the droplet's initial trajectory, there was some inherent error in this method due to each walker's unique interactions with the barriers of the launcher. We estimated this error to be  $0.05L$  by analyzing our trial videos for the maximum deviation from the theoretical impact parameter set by our droplet launcher.

### 4.3.2 Driving Acceleration

In order to measure the driving acceleration at which we were vibrating the fluid bath, we wired the accelerometer to the oscilloscope in order to return a wave function that we could analyze. We aimed to measure our driving acceleration through the quantity of path memory (Eq. 2.4) with the target of  $M = 0.99$ , the value used in Pucci et al.'s theoretical simulation. Since the driving acceleration is directly proportional to the amplitude of the vibration (Eq. 2.1), we only needed the fraction of the amplitude of our bath vibration over the amplitude of the Faraday threshold. The oscilloscope returned values of amplitude in intervals of 10 mV. We measured the driving acceleration to have an amplitude of 280 mV and the Faraday threshold to have an amplitude of 290 mV, resulting in a path memory value of  $M = 280/290 = 0.97 \pm 0.03$ . This was the largest value we could measure by putting the driving acceleration as close to the Faraday threshold as possible by slowly decreasing its amplitude with the function generator until no standing Faraday waves were visible.

### 4.3.3 Bath Depth

To create a bath depth of 6.42 mm, the bath depth used by Pucci et al., we filled the bath as close to the top of the 6 mm barriers as we could. We then measured out 5.84 mL of oil, which corresponded to 0.42 mm of bath depth in our bath size and added it to the bath. The error in measuring out the 5.84 mL of oil was negligible with respect to our bath depth. We did estimate an error of 0.1 mm in

our filling the bath to the top of the barriers as the characteristics of the oil made this alignment less than exact. Thus, our reported bath depth was  $6.4 \pm 0.1$  mm.

#### 4.3.4 Bath Lid

The purpose of the fluid bath lid is to protect the system from any ambient air currents present in the lab as Pucci et al. showed this can drastically alter the trajectory of a given walker. They investigated this effect by running trials both with and without a fluid bath lid and found that divergence from the droplet's initial trajectory was significantly enhanced with the introduction of ambient air currents. Their setup included a lid design that completely sealed their fluid bath, a design we did not have the resources to create. Thus, we designed a square-shaped Plexiglas lid that we mounted to hang over the edges of the fluid bath, but not completely seal it from external air currents. Thus, minor air currents may have affected the trajectory of our diffracted walkers. It is unknown what errors may have been introduced by these minor air currents.

#### 4.3.5 Tracker Measurement

We utilized Tracker video analysis software to measure each angle of diffraction as mentioned in Chapter 3. This required manually aligning a protractor with the walker's initial and final trajectories to determine the angle between as shown in Fig. 3.5. This included some error, as we could not align the protractor exactly to the walker trajectory, as well as the fact that the walker's final trajectory was not always straight making it somewhat ambiguous when aligning the protractor to it. We estimated this error to be  $5^\circ$  by taking different potential diffraction angle measurements from some abnormal droplet trajectories and seeing the maximum angle they differed by.

### 4.4 Deviations from Pucci et al. Study

While we aimed to replicate Pucci et al.'s study as closely as possible, we were forced to make some significant deviations from it due to limitations of both time and resources. These included a smaller bath diameter of 13.3 cm compared to theirs of 16 cm. We also used a smaller range of impact parameters. As shown in their compiled walker trajectories in Fig. 2.4, their various impact parameters virtually cover the entire width of the slit, while ours were varied in intervals of  $y/L = 0.2$ . This was in order to keep the number of setups and trials realistic and made our data less complete, most notably the two scatter plots. This made it difficult to discern trends from them since there are such large gaps between

each group of data points. We also included a different and smaller variety of slit widths in our study due to the size of our bath and limited time frame. Lastly, as mentioned in Sect. 4.3, our bath lid was not sealed, allowing minor air currents to potentially affect the walker trajectories. While the effects of these deviations are uncertain, they should be noted as potential causes of the difference between our data and that of Pucci et al.

## 5 Conclusion

Our study set out to investigate two conclusions of Pucci et al.'s study that we've continually referred back to:

1. Walker diffraction does not resemble Fraunhofer diffraction.
2. The diffraction angle of walkers is dependent on their impact parameter.

More specifically, we wanted to experimentally confirm whether or not these held true in systems of different slit widths, which their study simulated theoretically.

With regards to the first statement, our results showed that our walkers yielded diffraction patterns with minor similarities to Fraunhofer diffraction. There was resemblance with our  $L = 4\lambda_F$  slit width diffraction pattern that consisted of visible peak alignment, though the peak amplitudes were much greater than the peaks of the Fraunhofer curve. Our  $L = 8\lambda_F$  diffraction pattern also had pronounced peaks but resembled the Fraunhofer curve even less. After investigating these histograms in comparison to those of each impact parameter, we found that these peaks are likely a result of the dependence of the diffraction angle on the impact parameter as each  $y/L$  resulted in a concentration of data points at a certain  $\alpha$ , creating the peaks that are visible in the complete histograms for each slit width. This implies that these peaks are not a result of an interference effect similar to what results in Fraunhofer diffraction, but of an unforeseen consequence of varying the impact parameter in such large intervals, supporting the dependence of  $\alpha$  on  $y/L$  found by Pucci et al. Therefore, while our data refute the first statement, the minor resemblance to Fraunhofer diffraction is likely a coincidence and does not support the analogy suggested by Couder and Fort.

As for the second statement, our two scatter plots indicated two different conclusions. The scatter plot for our  $L = 4\lambda_F$  slit width indicated no dependence of the diffraction angle on the impact parameter, contrary to Pucci et al.'s findings. The scatter plot for our  $L = 8\lambda_F$  slit width contained an association of  $\alpha$  and  $y/L$  that was linear and oriented down and to the right. This matched the general,

negatively oriented trend of Pucci et al.’s data, though theirs was exponential while ours was linear. Thus, one of our slit widths had a diffraction pattern that indicated there is a dependence similar to what they found. This is contradicted by the lack of dependence in our other scatter plot for  $L = 4\lambda_F$ , but that is likely due to the fact that there is a smaller margin for error in smaller slit widths. Therefore, our impact parameter error may have skewed any potential dependence in that setup more so than in the  $L = 8\lambda_F$ . In conclusion, our data did not confirm the second statement for the smaller slit width, but did confirm it for the wider slit width.

Now that we have produced answers to these questions, we can finally return to the initial inspiration for this study: investigating whether or not this system can be used as a macroscopic model for quantum mechanics, specifically pilot wave theory. Our setup lacked the precision to expect to get results that closely matched the theoretical results of Pucci et al., but even so, our results contained multiple trends that aligned with their findings. Furthermore, the minor resemblance we found to Couder and Fort’s data we determined to be due to the dependence of  $\alpha$  on  $y/L$ . Thus, as our data were primarily supportive of Pucci et al., we have only cast further doubt on this system’s potential applications to understanding quantum mechanics. But, we acknowledge that the limited extent of our investigation leaves much parameter space to be explored that could possibly yield results that support this analogy first suggested by Couder and Fort.

## 5.1 Future Work

As our results did not experimentally confirm the results Pucci et al.’s study, there is much future work that could be done to attempt to do so. It would require taking a greater amount of data by varying the impact parameter in intervals that are more continuous than ours. It would also require collecting data from a wider variety of slit widths as our data did not cover the range that their theoretical study did. Lastly, in order to truly replicate the methods of Pucci et al., this work would require a more precise setup as it had numerous sources of error and deviations from their design that likely contributed to the differences in our data from theirs.

## Bibliography

- [1] Y. Couder and E. Fort, “Single particle diffraction and interference at a macroscopic scale,” *Phys. Rev. Lett.*, vol. 97, p. 154101, 2006.
- [2] R. D. Knight, *Physics - A Strategic Approach. Wave Optics*. Pearson Addison-Wesley, 2008.
- [3] J. W. M. Bush, “Pilot-wave hydrodynamics,” *Annu. Rev. Fluid Mech.*, vol. 47, pp. 269–292, 2015.
- [4] L. de Broglie, “La mecanique ondulatoire et la structure atomique de la matiere et du rayonnement,” *J. Phys. Radium*, vol. 8, pp. 225–241, 1927.
- [5] A. Z. Jones, “The Copenhagen Interpretation of Quantum Mechanics,” <https://www.thoughtco.com/copenhagen-interpretation-of-quantum-mechanics-2699346>, accessed: 2018-12-06.
- [6] G. Pucci, D. M. Harris, L. M. Faria, and J. W. M. Bush, “Walking droplets interacting with single and double slits,” *J. Fluid Mech.*, vol. 835, pp. 1136–1156, 2017.
- [7] S. Protiere, A. Boudaoud, and Y. Couder, “Particle-wave association on a fluid interface,” *J. Fluid Mech.*, vol. 554, pp. 85–108, 2006.
- [8] A. Eddi, E. Sultan, J. Moukhtar, E. Fort, M. Rossi, and Y. Couder, “Information stored in Faraday waves: The origin of a path memory,” *J. Fluid Mech.*, vol. 674, pp. 433–463, 2011.
- [9] M. B. Conner, “Tunneling in a Quantum Analog: An Experimental Investigation of a Bouncing Oil Droplet System,” 2015, undergraduate thesis - Reed College.
- [10] E. Hecht, *Optics*, 5th ed. Pearson, 2016.
- [11] D. J. Bohm and B. J. Hiley, “The de Broglie pilot wave theory and further development of new insights arising out of it,” *Found. of Phys.*, vol. 12, pp. 1001–1016, 1982.

- [12] D. M. Harris, T. Liu, and J. W. M. Bush, “A low-cost, precise piezoelectric droplet-on-demand generator,” *Exp. Fluids*, vol. 56, p. 83, 2015.
- [13] A. Mordvintsev and A. K., “Open CV - Python Tutorials: Hough Circle Transform,” <https://opencv-python-tutroals.readthedocs.io>.
- [14] D. Brown, “Tracker - Video Analysis and Modeling Tool,” <https://physlets.org/tracker/>.